Retrieval and characterization of ozone vertical profiles from a thermal infrared nadir sounder

Pierre-François Coheur, Brice Barret, Solène Turquety, Daniel Hurtmans, Juliette Hadji-Lazaro, Cathy Clerbaux

Retrieval and characterization of ozone vertical profiles from a thermal infrared nadir sounder

Pierre-François Coheur,[1] Brice Barret,[1] Solène Turquety,[2] Daniel Hurtmans,[1] Juliette Hadji-Lazaro,[2] and Cathy Clerbaux[1,2]

Received 27 February 2005; revised 15 September 2005; accepted 13 October 2005; published 17 December 2005.

[1] This paper presents the first retrievals and validations of ozone vertical distributions from a set of high-resolution nadir thermal infrared measurements. These were obtained by the Interferometric Monitor for Greenhouse gases (IMG) instrument, which has operated on board the Japanese ADEOS platform between 1996 and 1997. The Optimal Estimation Method is used for the retrievals, along with a priori profile and covariance matrix built from model climatologies. We compare the retrieved IMG profiles with high-vertical-resolution ozone sonde measurements. Therefore we selected a set of IMG spectra collocated to within 3° of longitude and latitude with a representative distribution of ground-based stations. We demonstrate that thanks to the two to four independent pieces of vertical information contained in the spectroscopic measurements with a maximum sensitivity in the upper troposphere–middle stratosphere, the thermal infrared nadir sounders are able to capture most of the ozone spatial and temporal variations. In particular, the latitudinal variations of the stratospheric ozone maximum are well represented in the retrievals, as are the high ozone concentrations observed in the upper troposphere–lower stratosphere at northern midlatitudes during springtime. Ozone depletion events in the Arctic vortex are also well reproduced. The measurements provide an accurate view of the tropospheric ozone content, except when the latter is very low. A detailed error budget reveals that the major part of the error in the IMG retrieved ozone profile is due to the smoothing of the true profile by the averaging kernel matrix, with additional contributions associated with the measurement noise and the inaccurate knowledge of the temperature profile and of the Instrument Line Shape (ILS).

Citation: Coheur, P.-F., B. Barret, S. Turquety, D. Hurtmans, J. Hadji-Lazaro, and C. Clerbaux (2005), Retrieval and characterization of ozone vertical profiles from a thermal infrared nadir sounder, *J. Geophys. Res.*, *110*, D24303, doi:10.1029/2005JD005845.

1. Introduction

[2] Ozone plays a key role in the chemical processes occurring in the atmosphere, as well as on the climate. On average, about 90% of the total ozone is present in the stratosphere and only 10% in the troposphere. Important variations of the ozone vertical distribution can, however, occur as a result of photochemical and dynamical processes. The tropospheric ozone component is particularly highly variable in space and time [*Lelieveld and Dentener*, 2000], and needs to be monitored as accurately as possible over the globe in order to provide a better insight into air quality, the transport of pollution or the radiative forcing.

[3] The measurement of the ozone vertical distribution in the lower atmosphere is best performed by ozone sondes, which generally provide values of ozone concentrations from the ground to about 30–35 km, with a very high vertical resolution (0.1 km) and a good precision (2%) and accuracy (5%). The Network for the Detection of Stratospheric Changes (NDSC) provides long time series of ozone sonde measurements, at different sites, mainly located in the Northern Hemisphere. The World Ozone and Ultraviolet Data Center (WOUDC) provides soundings at many additional locations, but the regular measurements in the Southern Hemisphere and tropical regions remained sparse until recently. The Southern Hemisphere Additional Ozonesondes (SHADOZ) program, which has archived data since 1997 [*Thompson et al.*, 2003a, 2003b, 2004], has therefore improved the spatial coverage of the ozone sonde network. In spite of this, the local sondes measurements, typically performed on a weekly basis, are not able to give a global picture of the changing ozone distribution and therefore to provide the required data to better understand tropospheric chemical and dynamical processes, and to track pollution events. Remote sensing from satellite-based instruments offers the best way to complement the ozone sonde measurements.

[4] In the past, the satellite remote sensing of ozone has mainly taken advantage of the strong spectral signatures that the molecule displays in the UV and the visible spectral regions. In particular, the Total Ozone Mapping

[1]Spectroscopie de l'Atmosphère, Service de Chimie Quantique et de Photophysique, Université Libre de Bruxelles, Brussels, Belgium.
[2]Service d'Aéronomie, Institut Pierre-Simon Laplace, Paris, France.

0148-0227/05/2005JD005845

Spectrometer (TOMS) (http://toms.gsfc.nasa.gov/) and the Global Ozone Monitoring Experiment (GOME) [*Burrows et al.*, 1999] have proven very valuable for measuring global ozone concentrations. With TOMS, quantitative information on the tropospheric ozone component was obtained by subtracting the ozone column above the tropopause, as measured by alternative satellites [e.g., *Fishman et al.*, 2003, and references therein]. The method proved very successful in identifying seasonal and spatial variations of tropospheric ozone, but showed limited accuracy when compared to ozonesondes in some cases [*Peters et al.*, 2004]. The retrieval of tropospheric ozone partial columns from the GOME instrument, which allowed measuring ozone profiles down into the troposphere, was successfully achieved by means of different algorithms [*Hoogen et al.*, 1999a, 1999b; *Müller et al.*, 2003; *Munro et al.*, 1998]. The results showed good agreement with the sondes and alternative satellite instruments in most cases.

[5] High-resolution nadir infrared spectroscopy from space offers another means for measuring accurate ozone concentrations on a global scale [*Clerbaux et al.*, 1998; *Turquety et al.*, 2002, 2004]. These measurements, which use the intense ozone absorption band around 10 μm, will gain importance on the short term with the launches of the Tropospheric Emission Spectrometer (TES, on board EOS-AURA) in June 2004 and the series of Infrared Atmospheric Sounding Interferometers (IASI, on board MetOp) from 2006. Interestingly, both platforms also include UV-visible instruments (OMI and GOME-2, respectively), which could be used in synergy with the infrared spectrometers to improve the accuracy as well as the vertical sensitivity of the ozone retrievals. In order to investigate this further, it is at first important to fully characterize the information that can be extracted for the ozone vertical distribution with each of these instruments taken individually. This work aims at performing a detailed study regarding the potential of high-resolution nadir spectrometers operating in the thermal infrared spectral range, to measure ozone vertical profiles. Such analyses have been conducted previously for the preparation of the TES mission [*Bowman et al.*, 2002; *Clough et al.*, 1995]. In their paper, Bowman et al. have notably demonstrated, on the basis of simulated spectra from ozone sonde measurements over a single location (the Bermuda), that the IR nadir sensors should be able to capture large ozone variations in the troposphere, with a resolution of about 6 km. In this work, we intend to go further, by analyzing a set of data from the Interferometric Monitor for Greenhouse gases (IMG) instrument [*Kobayashi et al.*, 1999], which flew on board the Japanese ADEOS platform between 1996 and 1997. IMG provided the first set of high-resolution nadir thermal infrared spectra, especially well suited to evaluate the scientific return to be expected from forthcoming satellite missions.

[6] In the next section, the IMG instrument and spectra are briefly presented. Section 3 describes the retrieval approach and algorithm as well as the characterization methods used, in terms of information content and error analysis. Section 4 presents the results of the ozone retrievals, made on a selection of IMG spectra, coincident with ozone soundings made at several stations around the globe. Relying on the comparison with the sondes data, the discussion emphasizes the accuracy of the retrieved profiles and partial columns, as a function of the different sources of errors and the vertical sensitivity. Section 5 summarizes the study and puts forward some perspectives.

2. IMG Instrument and Spectra

[7] The IMG instrument was developed under the initiative of the Japanese Ministry of International Trade and Industry (MITI), to be part of the ADEOS sun-synchronous, ground track repeat, polar-orbiting satellite.

[8] The IMG mission aimed at measuring the distributions of the main atmospheric greenhouse gases from space. To reach these objectives, the instrument was chosen to be a high spectral resolution (10 cm Maximum Optical Path Difference) Fourier transform spectrometer, operating in three separate bands, extending from 2387 to 3030 cm^{-1} (band 1), 2000 to 2500 cm^{-1} (band 2) and 600 to 2000 cm^{-1} (band 3). The Field Of View (FOV) was defined by the size of the detectors as three squares of 8 km × 8 km footprint on the ground [*Kobayashi et al.*, 1999]. Radiometric performances on flight satisfied the designed and scientific requirements in bands 2 and 3 but band 1 failed to reach the specifications in terms of signal-to-noise ratio.

[9] As a result of the arrangement of the detectors (band 2 being at the center of the FOV while band 1 and 3 were slightly off axis), the Instrumental Line Shape (ILS) in the band 3 of interest to this work, is broadened not only by FOV effects but also by the impact of off-axis incident light into the instrument. We have used the formulation of *Kauppinen and Saarinen* [1992] to model this distortion but additional broadening of the ILS proved necessary to reproduce the measurements around 10 μm, as shown by the spectral fit of CO_2 lines laying on both sides of the ozone band (Figure 1). This leads to a total ILS with a Full Width at Half Maximum (FWHM) of 0.19 cm^{-1} at 1000 cm^{-1}.

[10] Because of the huge flow rate of data, IMG operations were limited to periods of four successive days, except for one specific period of 10 days, 1–10 April 1997. Furthermore, the data were recorded as series of six measurements, each separated by 86 km along the track, followed by deep space observations and internal blackbody calibrations. These constraints, combined with the short lifetime of the mission (August 1996 to June 1997), resulted in a relatively limited number of high-quality nadir infrared spectroscopic measurements from space. Studies on the IMG spectra have been successfully undertaken to retrieve global columnar abundances of several species (O_3, CO, CH_4) [*Clerbaux et al.*, 1998, 1999, 2001, 2003; *Hadji-Lazaro et al.*, 1999; *Turquety et al.*, 2002, 2004]. Other species show absorption bands in the IMG spectra (e.g., CO_2, N_2O, HNO_3, CFC-11, CFC-12) [*Chédin et al.*, 2003; *Clerbaux et al.*, 2003; *Coheur et al.*, 2003; *Lubrano et al.*, 2002], though for those no retrievals have yet been reported.

3. Retrieval Method and Data Analysis

[11] The results presented in this work were obtained using the *Atmosphit* software, recently developed at the Université Libre de Bruxelles [*Barret et al.*, 2005].

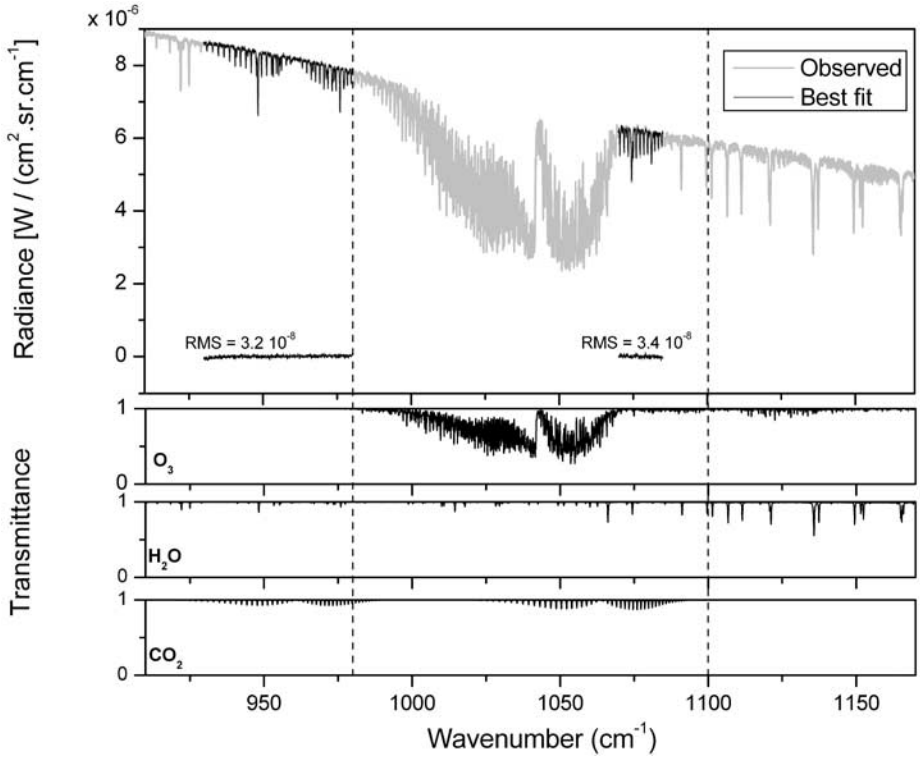

Figure 1. Portion of an IMG spectrum in band 3 (shaded line) around the ozone band at 10 μm. The solid spectrum gives the spectral fit using the modeled ILS in two microwindows dominated by CO_2 absorption lines. The residual spectrum and the associated RMS are also provided. The bottom plots give the individual contributions due to O_3, H_2O and CO_2. The dotted lines indicate the limits of the spectral range considered for the ozone profile retrievals.

3.1. Forward Modeling

[12] Given an a priori atmosphere divided in discrete levels, the general forward radiative transfer equation can be written as

$$\mathbf{y} = \mathbf{F}(\mathbf{x}, \mathbf{b}) + \boldsymbol{\varepsilon} \tag{1}$$

where $\mathbf{y}$ is the measurement vector containing measured radiances, $\mathbf{x}$ is the concentration profile to be retrieved and $\mathbf{b}$ represents all other model parameters having an impact on the measurement. ε is the measurement noise and $\mathbf{F}$ is the forward radiative transfer function.

[13] In *Atmosphit*, a synthetic spectrum is computed from equation (1) using the line parameters (positions, intensities, broadening and shifting parameters, including their dependence on temperature), and absorption cross sections for the heavier molecules, as collected in spectroscopic databases (e.g., HITRAN [*Rothman et al.*, 2003] or GEISA [*Jacquinet-Husson et al.*, 1999]). The water vapor, carbon dioxide, oxygen and nitrogen continua are also included. For water vapor, the recently issued MT-CKD model is chosen [*Clough et al.*, 2005]. For the molecular lines, a Voigt line shape is used in each atmospheric layer. The resulting spectrum is then processed to account for the ILS, including the eventual distortion generated by straight and tilted FOV effects.

3.2. Retrieval Concept

[14] The goal of the retrieval is to find the state vector $\hat{\mathbf{x}}$, an approximate of the true state $\mathbf{x}$, that is most consistent with the measurement and a priori information. The specific problem of retrieving vertical profiles from nadir spectra, which provide an integrated view of the atmosphere, is ill conditioned and has no unique solution. The retrievals need therefore to be regularized in order to produce meaningful results. In the *Atmosphit* software, this is done using the Optimal Estimation Method (OEM) [*Rodgers*, 2000]. In the OEM formalism, the inverse problem can be written as

$$\hat{\mathbf{x}} = \mathbf{R}\left(\mathbf{y}, \hat{\mathbf{b}}, \mathbf{x_a}, \mathbf{S}_a, \mathbf{S}_\varepsilon\right) \tag{2}$$

where $\mathbf{x_a}$ is the a priori profile and $\hat{\mathbf{b}}$ is an estimate of the model parameters $\mathbf{b}$, including, e.g., pressure, temperature and other gases volume mixing ratios. $\mathbf{S}_a$ and $\mathbf{S}_\varepsilon$ are the a priori and measurement covariance matrices, respectively. $\mathbf{R}$ is the inverse transfer function.

[15] In this study, a priori information for ozone volume mixing ratio was built as in the work by *Turquety et al.* [2004], considering the Model for Ozone and Related chemical Tracers climatologies (MOZART) [*Brasseur et al.*, 1998; *Hauglustaine et al.*, 1998] for the volume mixing ratios up to the tropopause and from the monthly satellite 4D ozone climatology from *Li and Shine* [1995] higher up. A single a priori profile was used for all retrievals: It is a globally averaged profile, defined by layers of 1 km from the ground up to 100 km and generated by considering two profiles per month on the $2.8 \times 2.8°$ MOZART grid. The a priori covariance matrix $\mathbf{S_a}$ was generated from the same set of vertical profiles and thus represents the yearly spatial and temporal variability of ozone. The measurement covariance matrix $\mathbf{S}_\varepsilon$ was chosen to be diagonal with identical σ_ε^2

diagonal elements characterized by $\sigma_\varepsilon = 1 \times 10^{-7}$ W/(cm^2.sr.cm^{-1}). The σ_ε value, which accounts for all the systematic sources of errors including the radiometric noise, was adjusted on a sample of spectra such as to minimize undesired oscillations in the retrieved vertical profiles, while providing a good spectral fit and keeping the relevant information from the measurements.

[16] In the case of a moderately nonlinear problem, the solution of equation (2) is found by iteration of:

$$\hat{\mathbf{x}}_{i+1} = \mathbf{x}_a + \left(\mathbf{K}_i^T \mathbf{S}_\varepsilon^{-1} \mathbf{K}_i + \mathbf{S}_a^{-1}\right)^{-1} \mathbf{K}_i^T \mathbf{S}_\varepsilon^{-1} \cdot [\mathbf{y} - \mathbf{F}(\hat{\mathbf{x}}_i) + \mathbf{K}_i(\hat{\mathbf{x}}_i - \mathbf{x}_a)], \quad (3)$$

which introduces the Jacobian matrix $\mathbf{K} = \partial\mathbf{y}/\partial\mathbf{x}$, the rows of which are the partial derivatives of the measurement with respect to the retrieved variables. The retrieved state is obtained after convergence, when the absolute difference between every element of $\mathbf{F}$ modeled at the two last iteration steps, $|\mathbf{F}(\mathbf{x}_i + 1) - \mathbf{F}(\mathbf{x}_i)|$, is less than a fraction (20%) of σ_ε.

3.3. Characterization of the Retrievals and Error Analysis

[17] The characterization of the information contained in the measurements and the computation of the error sources are essential to access the potential of remote sensing instruments to probe the atmospheric composition. The characterization is performed relying on the linear approximation, as formalized by *Rodgers* [2000]. In such case, the retrieved state is given by:

$$\hat{\mathbf{x}} = \mathbf{x}_a + \mathbf{A}(\mathbf{x} - \mathbf{x}_a) + \mathbf{G}\left(\varepsilon + \mathbf{K}_b\left(\mathbf{b} - \hat{\mathbf{b}}\right)\right), \quad (4)$$

where $\hat{\mathbf{b}}$ are the approximate of the model parameters $\mathbf{b}$ and $\mathbf{K}_b = \partial\mathbf{F}/\partial\mathbf{b}$. $\mathbf{G}$ and $\mathbf{A}$ are the gain and averaging kernel matrices, respectively, defined by:

$$\mathbf{G} = \frac{\partial\hat{\mathbf{x}}}{\partial\mathbf{y}} \quad (5)$$

$$\mathbf{A} = \frac{\partial\hat{\mathbf{x}}}{\partial\mathbf{x}} = \mathbf{GK} \quad (6)$$

[18] The averaging kernels provide an interesting measure of the sensitivity of the retrieved state to the true state: At a given level, the peak of the averaging kernel gives the altitude of maximum sensitivity whereas its full width at half maximum can be interpreted as the vertical resolution of the retrieval. The vertical sensitivity of the retrievals can also be evaluated by means of the information content (H) or the degrees of freedom for signal (hereafter DOFS or d_s). H represents the reduction in entropy of a probability density function (in our case the knowledge of the ozone vertical distribution) before and after the measurements, whereas d_s is an estimate of the number of independent pieces of information contained in the measurements [*Rodgers*, 2000]. They are calculated as:

$$H = \frac{1}{2}\sum_i \ln\left(1 + \lambda_i^2\right) \quad (7)$$

$$d_s = \sum_i \lambda_i^2/\left(1 + \lambda_i^2\right) = tr(\mathbf{A}) \quad (8)$$

where the λ_i are the singular values of $\tilde{\mathbf{K}} = \mathbf{S}_\varepsilon^{-\frac{1}{2}}\mathbf{K}\,\mathbf{S}_a^{\frac{1}{2}}$.

[19] The error on the retrieved quantity can be calculated as the difference between the retrieved state and the true state. From (4) one has:

$$\hat{\mathbf{x}} - \mathbf{x} = (\mathbf{A} - \mathbf{I})(\mathbf{x} - \mathbf{x}_a) + \mathbf{G}\varepsilon + \mathbf{GK}_b\left(\mathbf{b} - \hat{\mathbf{b}}\right) \quad (9)$$

It follows from the right-hand side of equation (9) that the total error decomposes into different contributions, related respectively to the smoothing error, which accounts for the sensitivity of the measurements to the vertical structure of the atmospheric variable to be retrieved, the measurement error and the forward model parameters error. Their covariances are calculated as

$$\mathbf{S}_{smoothing} = (\mathbf{A} - \mathbf{I})\mathbf{S}_a(\mathbf{A} - \mathbf{I})^T \quad (10)$$

$$\mathbf{S}_{meas.} = \mathbf{GS}_n\mathbf{G}^T \quad (11)$$

$$\mathbf{S}_{\mathrm{mod}.param.} = \mathbf{GK}_b\mathbf{S}_b(\mathbf{GK}_b)^T \quad (12)$$

The computation of the first error term calls for the previously defined $\mathbf{S}_a$ covariance matrix. In equation (11) $\mathbf{S}_n$ is a covariance matrix representative of the true measurement error. It is taken diagonal, with elements being the variances of the radiometric noise. The $\mathbf{S}_b$ covariance matrices used to compute the errors due to uncertainties on the model parameters are also assumed to be diagonal. The total error covariance is obtained by summing the individual contributions:

$$\mathbf{S}_{total} = \mathbf{S}_{smoothing} + \mathbf{S}_{meas} + \mathbf{S}_{mod.param.} \quad (13)$$

3.4. Application to the Analysis of the IMG Data

[20] In the retrievals, the entire ozone band between 980 and 1100 cm^{-1} was considered, without gaps. This spectral region encompasses most of the strong ozone absorption lines in the thermal infrared and is also relatively free of other interfering gases, with the presence of only some lines of H_2O and CO_2 (Figure 1). The CO_2 profile was kept constant in the retrieval whereas ozone was fitted along with surface temperature and water vapor column. The ozone volume mixing ratios (vmr's) were retrieved in 1 km thick layers from the ground to 60 km and in two additional 20 km thick layers at higher altitudes.

[21] Additional input parameters include the pressure and the temperature profiles. These were taken from the European Center for Medium Range Weather Forecasts (ECMWF) and were interpolated to the date and location of the IMG measurements. The spectroscopic parameters were extracted from the recently issued GEISA-IASI 2003 database [*Jacquinet-Husson et al.*, 2005], which contains important updates for ozone in the infrared.

[22] A set of clear-sky spectra [*Hadji-Lazaro et al.*, 2001] colocated to within 3° of longitude and latitude with seven NDSC or WOUDC stations representative of different latitudes, embracing polar, midlatitudes and tropical regions, and providing high-vertical-resolution ozone soundings, has been considered (Table 1). The temporal

Table 1. Summary of the Coincident IMG and Ozone Sonde Measurements

Observing Site, Latitude, Longitude, Altitude Above Sea Level	Period of O_3 Sonde Measurement	Number of Sonde Data	Number of Coincident IMG Measurements
Ny Alesund, 78.92°, 11.93°, 15 m	January 1997	2	10
Ny Alesund, 78.92°, 11.93°, 15 m	February 1997	1	2
Ny Alesund, 78.92°, 11.93°, 15 m	March 1997	1	2
Ny Alesund, 78.92°, 11.93°, 15 m	April 1997	3	4
Uccle, 50.80°, 4.35°, 100 m	March 1997	1	4
Uccle, 50.80°, 4.35°, 100 m	April 1997	1	4
Uccle, 50.80°, 4.35°, 100 m	June 1997	2	4
Wallops, 37.94°, −75.46°, 7m	April 1997	1	3
Wallops, 37.94°, −75.46°, 7m	June 1997	1	5
Hilo, 19.72°, −155.07°, 11 m	April 1997	1	2
Easter Island, −27.17°, −109.42°, 69 m	January 1997	1	6
Easter Island, −27.17°, −109.42°, 69 m	June 1997	1	5
Lauder, −45.04°, 169.68°, 370 m	December 1996	1	2
Lauder, −45.04°, 169.68°, 370 m	March 1997	1	6
Lauder, −45.04°, 169.68°, 370 m	April 1997	2	5
Lauder, −45.04°, 169.68°, 370 m	May 1997	1	3
Neumayer, −70.65°, −8.26°, 42 m	January 1997	1	3
Neumayer, −70.65°, −8.26°, 42 m	April 1997	1	1

coincidence criterion was one day. This provided us with an ensemble of 23 sonde measurements and 69 coincident clear-sky IMG observations, during a period extending from December 1996 to June 1997. The sonde measurements, which are performed at a very high vertical resolution, need to be smoothed in order to account for the lower resolution of the IMG observing system and thus to allow a meaningful comparison with the retrieved ozone profiles. The smoothed ozone sonde profiles $\mathbf{x}_s$ are calculated from the measured profiles $\mathbf{x}_{sonde}$ according to [*Rodgers*, 2000]:

$$\mathbf{x}_s = \mathbf{x}_a + \mathbf{A}(\mathbf{x}_{sonde} - \mathbf{x}_a) \quad (14)$$

4. Results and Discussion

4.1. Retrieval and Characterization of the Ozone Profile

[23] Examples of spectral fits and of the associated retrieved ozone profiles are provided in Figure 2, for measurements colocated above the Uccle and Ny-Alesund stations. In both cases, the fit of the ozone band is satisfactory, with the residuals being somewhat larger than the one obtained for the fit of CO_2 lines laying on both sides, but close to the σ_ε value selected to constrain the retrievals (Figure 1). Fits achieve χ^2 values of 0.7 and 0.2, which is indicative of the conservative approach used in the choice of σ_ε.

[24] For the two examples, the retrieved ozone profiles are in good agreement with the sonde measurements, over the entire altitude range covered by the latter (Figure 2b): The relative differences calculated with respect to the ozone sondes, smoothed according to equation (14), do not exceed 50% in the altitude range investigated. In particular, the retrievals provide a very good representation of typical structures in the ozone profile, such as the lower height of the stratospheric ozone maximum in Ny-Alesund and the presence of a secondary ozone maximum in the upper troposphere–lower stratosphere at Uccle. The higher ozone contents found at northern midlatitudes is well known and likely due to a combination of increased photochemistry and of the downward transport of ozone-rich air, from the stratosphere to the troposphere, which reaches a maximum in late winter and early spring [*Lelieveld and Dentener*, 2000].

[25] Further illustration of the potential of the thermal infrared nadir measurements to capture some fine variations of the ozone vertical distribution is given in Figure 3, which shows the retrieval result for an IMG measurement made within the Arctic vortex on 2 April 1997. The ozone column for this particular measurement is lower than usual for the region and the associated profile is characterized by a typical decrease of the ozone amount in the 12–24 km altitude range. The latter is due to the very low-stratospheric temperatures observed until the beginning of April 1997 in the Arctic, which enabled the formation of polar stratospheric clouds and thereby activated the chlorine chemistry [*Coy et al.*, 1997]. Very similar observations of the ozone depletion were made with the GOME instrument on the same day [*Eichmann et al.*, 1999; *Hoogen et al.*, 1999b].

[26] For the measurements depicted in Figure 2, which correspond to surface temperatures of 255 K at Ny-Alesund and 280 K at Uccle, d_s values of 2.9 and 3.3 are respectively calculated. This suggests that these measurements contain about three independent pieces of information on the vertical distribution of ozone. More generally, as demonstrated earlier by the analysis of the MOPITT CO measurements [*Deeter et al.*, 2004], it is expected that the information increases with increasing surface temperature. For the present ozone retrievals, which cover a range of surface temperatures between 220 and 300 K, this relationship is depicted in Figure 4: It is seen that the DOFS at the different stations and dates varies almost linearly with temperature, between 2.2 (polar regions in winter) and 3.9 (tropical regions).

[27] Figure 5 provides a detailed insight on the sensitivity of the measurements to the O_3 vertical distribution. In Figure 5, the averaging kernels for 6 km thick partial columns from the ground to 30 km are given for three reference cases, characterized by high (d_s = 3.9, H = 11.0), medium (d_s = 3.3, H = 8.3) and low (d_s = 2.9, H = 6.4) sensitivities. The analysis reveals that the information is, in

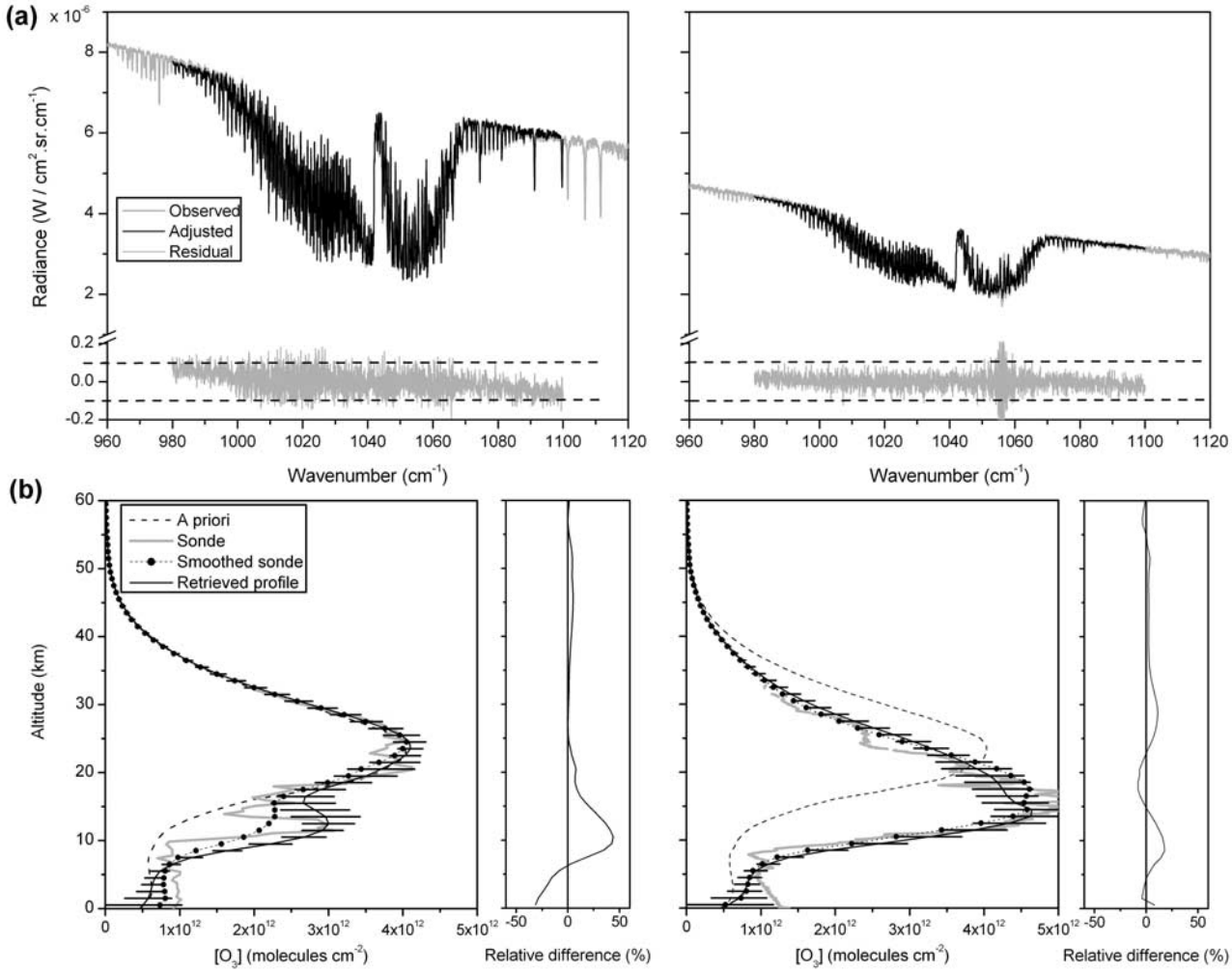

Figure 2. (a) Best ozone spectral fits for IMG observations above the Uccle (left plot) and Ny-Alesund (right plot) sites. The selected scenes correspond to surface temperatures of 280 and 255 K, respectively. The dashed lines at $\pm 10^{-7}$ W/(cm^2 sr cm^{-1}) correspond to the σ_ε value selected to constrain the retrievals. (b) Retrieved ozone profiles in number density units and relative differences calculated with respect to the smoothed ozone sonde profiles at the two locations. The a priori profile is also shown.

all cases, maximum from the middle troposphere to the middle stratosphere. In the most favorable situation (Figure 5, left), this information can be represented by three prominent averaging kernels, corresponding to the 6–12, 12–18 and 18–24 km partial columns, with an additional component (0–6 km) that brings some information down to the surface and a broad component that extends the sensitivity toward higher altitudes. The decrease of the information content characterizing the other two cases (Figure 5, middle and right), affects on the one hand the two stratospheric components, which broaden and begin to overlap each other, and on the other hand the sensitivity to the boundary layer. On the contrary, the averaging kernel for the middle troposphere (6–12 km) is weakly affected and becomes the dominant contribution to the integrated measurement response.

[28] The present analysis of the information content shows similarities with the results obtained by *Bowman et al.* [2002] for simulated measurements corresponding to the characteristics of the TES instrument. For the latter, which has a nominal resolution of 0.1 cm^{-1}, a better vertical resolution and an improved sensitivity on ozone in the 1 to 4 km altitude range are, however, expected.

[29] The error analyses, an example of which is provided in Figure 6, confirm that the retrievals are mainly driven by a priori information below 5 km and above 40 km. The ratio of the variability (square root of the $\mathbf{S}_a$ diagonal elements) to the total error (square root of the $\mathbf{S}_{total}$ diagonal elements), which indicates the extent of information that the measurements add to the a priori ozone profile (i.e. the reduction of the uncertainty on the ozone profile provided by the retrievals), varies between 1.3 and 3.7 in the 5–40 km altitude range. It is always greater than 2 above 7 km and reaches the highest values in the upper troposphere and the lower stratosphere. Figure 6 also shows that the smoothing error is the dominant error. Additional significant contributions include the measurement error, as well as the errors introduced by the inaccurate knowledge of the temperature profile and of the ILS (2 K and 2% variances on these quantities were respectively considered in the computation of equation (12)). The individual errors due to the surface properties (temperature and emissivity) and to the humidity

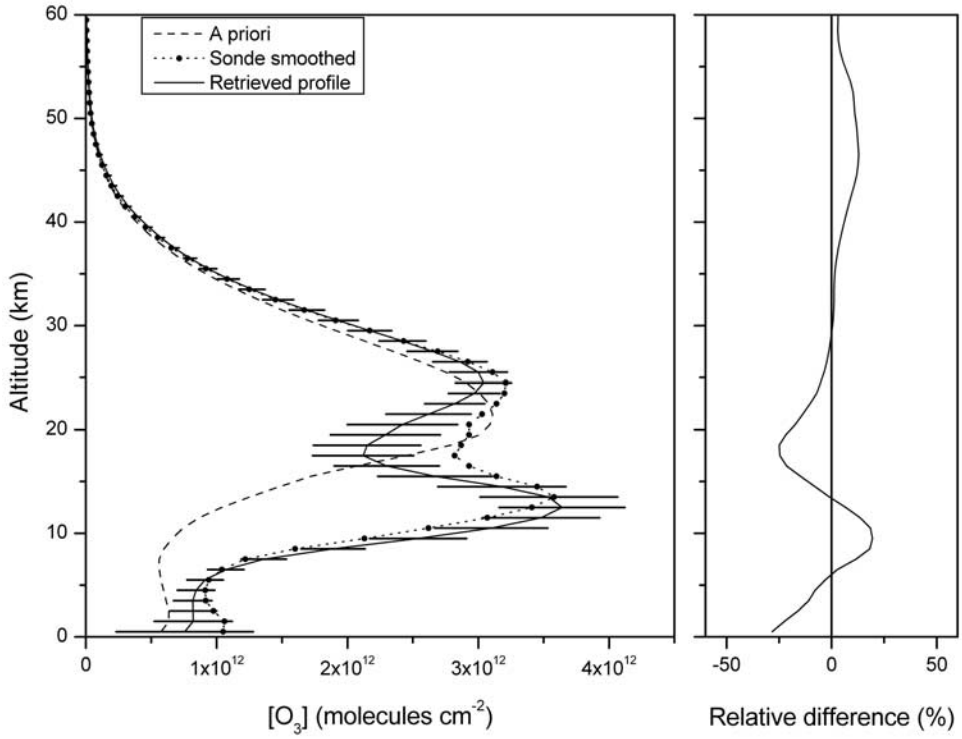

Figure 3. Retrieved ozone profile from an IMG observation made on 2 April 1997 in the Arctic Vortex and comparison with an ozone sonde measurement at Ny-Alesund.

profile are found to be lower than 5% and are not shown in Figure 6. The same conclusions hold for the different locations investigated here. Indeed, it is generally found that the total error varies between about 25 and 50% but that it is two to three times smaller than the a priori variability. The error is maximum around 10 km as a result of the tropopause variability. Interestingly, the most variable sources of error are those due to the upper-air temperature profile and to the ILS. The specific retrieval problems that are due to the poor characterization of the instrumental contribution

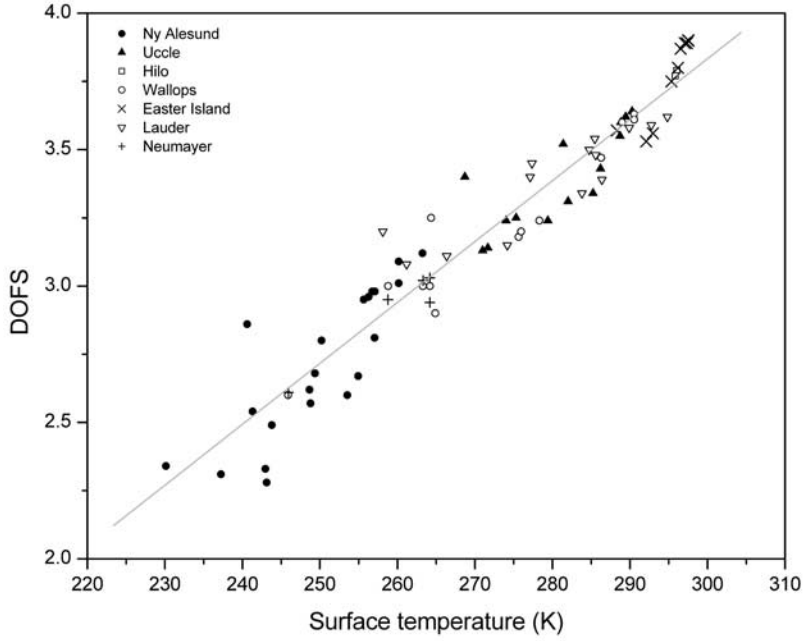

Figure 4. Degrees of freedom for signal (DOFS) calculated for ozone at the different observing sites and dates, as a function of the retrieved surface temperature. The shaded line shows a linear regression between all points.

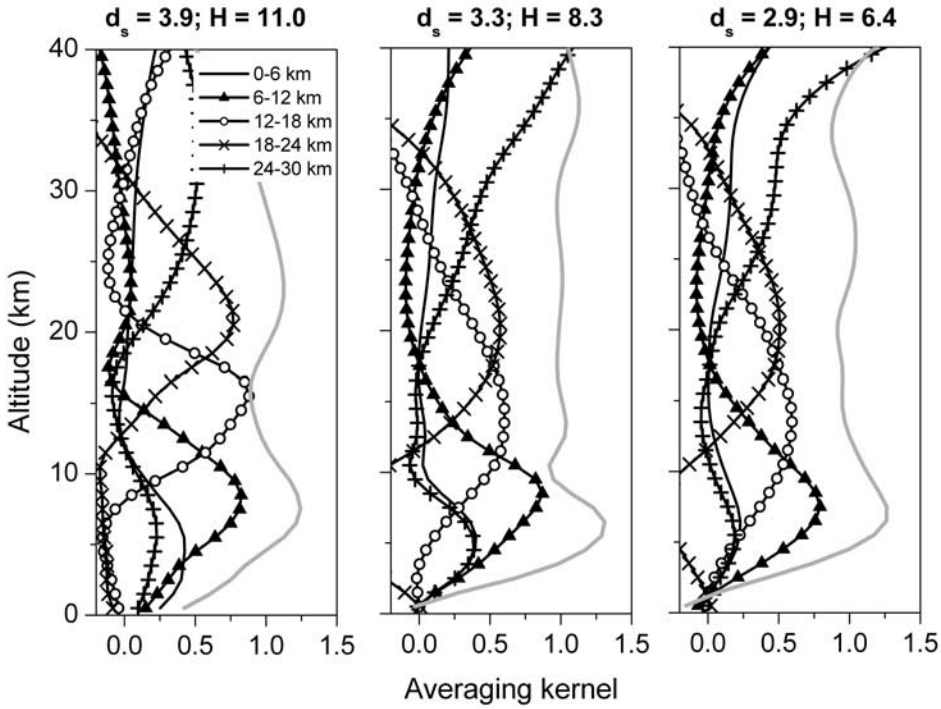

Figure 5. Averaging kernels for the 0–6, 6–12, 12–18, 18–24 and 24–30 km partial columns, for measurements made at (left) Easter Island, (middle) Uccle and (right) Ny Alesund. The shaded line plots the integrated measurement response. The DOFS (d_s) and information content (H) values are given at the top of each plot.

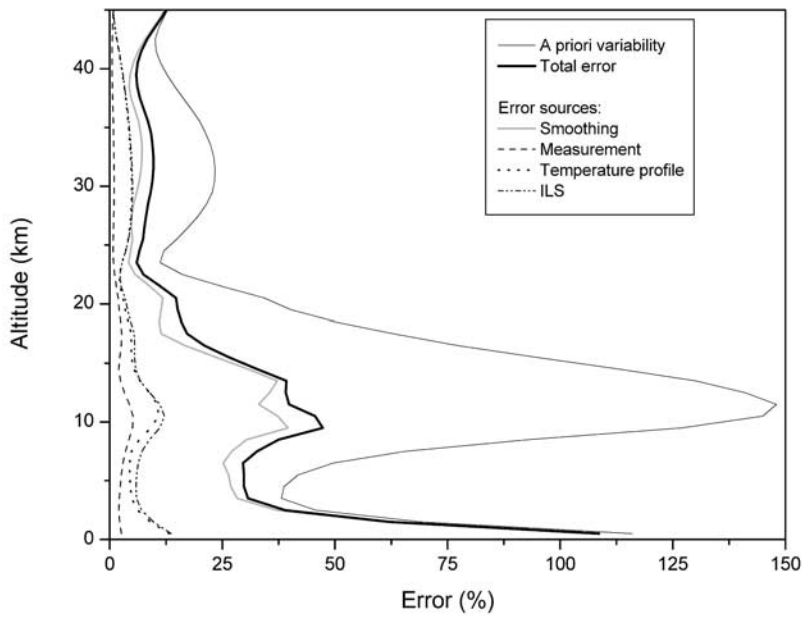

Figure 6. Error sources as a function of altitude for a retrieval at Ny-Alesund. The errors are the square root of the diagonal elements of the error covariance matrix (equations (10)–(13)) and of the a priori covariance matrix, respectively. The errors due to the surface properties (surface temperature and emissivity) and to the humidity profile, which contribute only weakly, are not shown. The a priori variability is given for comparison.

Table 2. Globally Averaged Ozone Partial and Total Columns (DU) at Each Observing Site[a]

	Ground to 12 km			12–24 km			24–30 km			Total		
	$[O_3]$ (DU)			$[O_3]$ (DU)			$[O_3]$ (DU)			$[O_3]$ (DU)		
Observing Site	Sonde	Retrieval	Bias (1σ)	Sonde	Retrieval	Bias (1σ)	Sonde	Retrieval	Bias (1σ)	Sonde	Retrieval	Bias (1σ)
Ny Alesund	64.3	67.5	4.6(23.2)	213.8	207.6	1.3(10.5)	45.0	40.6	−16.9(25.5)	···	341.9	...
Uccle	46.5	43.3	−2.4(36.9)	121.2	136.4	−0.4(7.3)	81.4	70.8	−0.4(11.7)	318.4	317.6	−0.8(8.8)
Wallops	45.4	50.1	10(12.0)	127.0	119.9	−6.0(9.8)	92.1	92.7	−0.2(5.4)	325.8	336.8	3.3(4.1)
Hilo	47.1	52.8	12.2(1.7)	90.7	87.8	−3.2(10.1)	94.5	94.7	0.2(3.3)	···	312.7	...
Easter Island	23.4	34.2	47.6(12.5)	71.0	65.0	−7.5(8.4)	78.9	87.5	10.3(4.7)	···	260.5	...
Lauder	25.3	39.0	58.5(37.8)	108.6	102.6	−7.5(12.1)	75.2	82.4	9.4(9.2)	272.9	292.4	6.9(9.3)
Neumayer	34.6	38.0	−7.3(9.9)	154.3	183.9	4.4(1.6)	47.3	44.0	−0.4(14.1)	···	274.9	...

[a]The bias and the 1σ standard deviation are given in percents.

in the IMG spectra were highlighted earlier by *Clerbaux et al.* [2002].

4.2. Validation of the Retrieved Profiles With Respect to the Sonde Data Set

[30] In light of the above conclusions, and in order to perform a statistical comparison between the ozone profiles retrieved from the satellite measurements and the local measurements provided by the sondes, we have calculated three partial columns, corresponding to the merged 0–12 (troposphere), 12–24 (lower stratosphere) and 24–30 km layers. The 30 km upper limit was chosen to include all sonde data. The partial columns from de sondes profiles, smoothed by the averaging kernels, have been considered in the comparison. The results are presented in Table 2 and in Figure 7. Table 2 also includes the comparison of the total column of ozone with that measured by the Dobson instruments, when available.

[31] In most of the cases, it is observed that the retrieved tropospheric ozone values, from the ground up to 12 km, are overestimated with respect to the sonde data (positive bias of 21%). This is especially true in the Southern Hemisphere

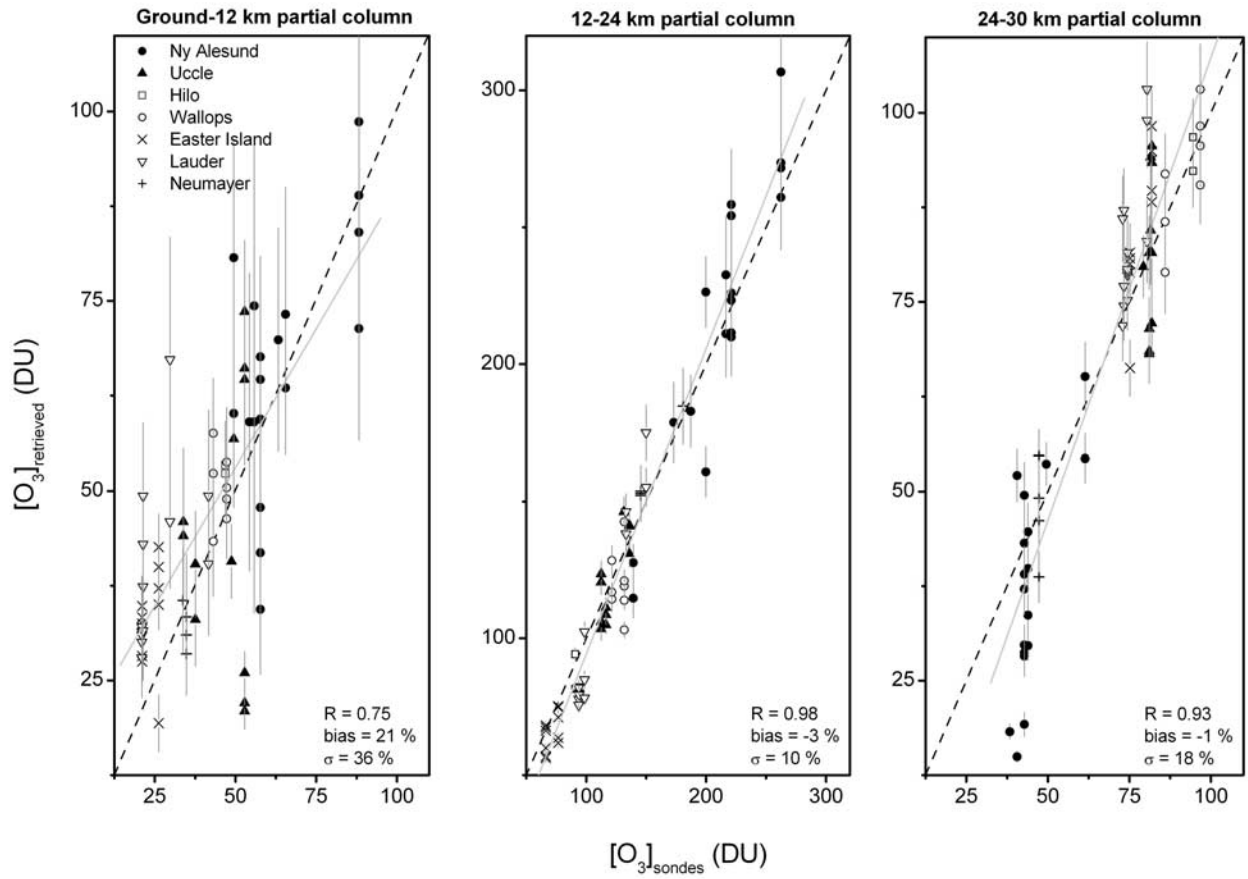

Figure 7. Scatterplots of the three retrieved partial columns (ground to 12 km, 12–24 km, and 24–30 km) versus the smoothed ozone sondes. The shaded lines show the linear regressions between all data points; the corresponding regression coefficient (R), bias and standard deviation (1σ) are also given. The dotted line, of unity slope, is shown for comparison.

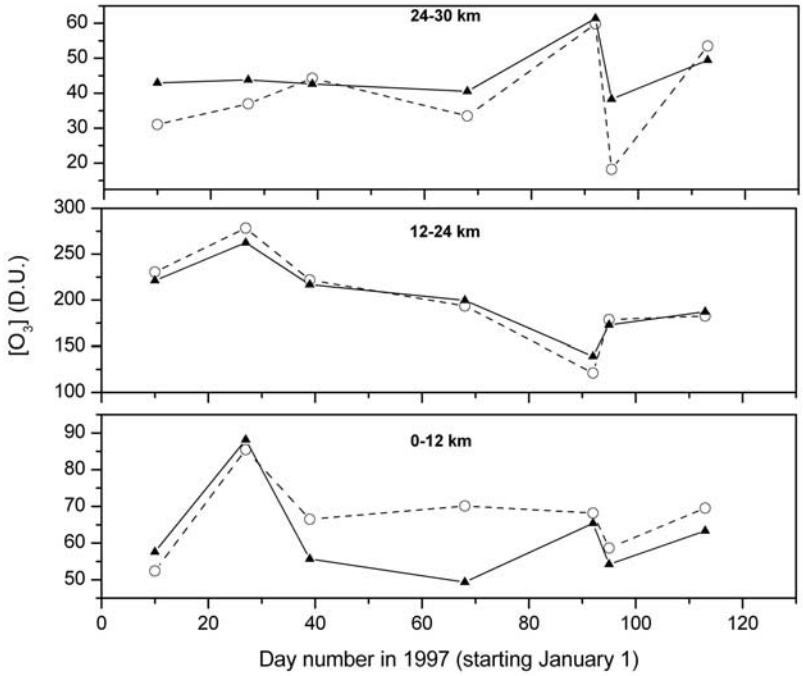

Figure 8. Temporal evolution of the ozone partial columns at Ny-Alesund between 10 January and 23 April 1997 for the colocated sonde and IMG measurements. The IMG retrievals and the sonde data are given by the open circles and solid triangles, respectively.

tropical (Easter Island) and midlatitude (Lauder) regions, which are characterized by the lowest-tropospheric ozone contents (~25 DU). With the exception of these two particular sites, the overall bias for the ground to 12 km partial column decreases to 4%, thereby highlighting the potential of the infrared remote sensor to sound ozone into the troposphere. The remaining disagreement between the satellite derived values in the troposphere and the sonde data can be explained, in part, by the limited sensitivity of the thermal IR nadir measurements toward the boundary layer, as discussed previously. The systematic errors due to, e.g., the ILS definition and the temperature profile, which are largest around the tropopause, also contribute to the discrepancies observed. Finally, it has to be kept in mind that the coincidence criteria selected are not optimal to perform an accurate comparison of the rapidly changing tropospheric ozone content.

[32] The retrieved lower-stratospheric partial columns (12–24 km) are in excellent agreement with the sonde data (correlation coefficient of 0.98), allowing to reproduce both the low and the high ozone concentrations in that altitude region. The comparison suggests, however, a slight tendency of the retrievals to underestimate the 12–24 km partial column, except in the polar region. Also the 24–30 km partial column is accurately retrieved from the IMG spectra in most cases (correlation of 0.93). These results open promising perspectives to study, with future sounders, Stratosphere-Troposphere Exchanges (STE) for ozone on the global scale. This is essential to discriminate the relative contribution of this process relative to others (pollution and burning sources, long-range transport, photochemistry) in the regulation of the tropospheric ozone content.

[33] The results demonstrate finally the ability of the nadir sounders to capture temporal variations of ozone in the troposphere and the stratosphere, in addition to the spatial variations. This is best seen with the retrieval results obtained over Ny-Alesund, which include 7 days of IMG measurements within a period extending from January to the end of April 1997 (Figure 8). The ozone depletion within the Arctic vortex, which is observed in the lower stratosphere in springtime, appears clearly in Figure 8.

4.3. Toward a Synergetic Use of Infrared and UV-Visible Measurements From Space

[34] The AURA and MetOp platforms carry both infrared and UV visible instruments, which will simultaneously measure ozone. Their sensitivity to the ozone vertical distribution is, however, different. From the analysis of the GOME measurements, the maximum sensitivity is found in the stratosphere, with a resolution between 5 and 9 km [*Hoogen et al.*, 1999b; *Munro et al.*, 1998]. Outside this altitude range, the resolution decreases to 10 km. Hoogen et al. also show that the tropospheric ozone component retrieved from the UV-visible measurements is moderately correlated to the ozone content in the lower stratosphere. The ozone profile retrievals from GOME using either the optimal estimation method [*Hoogen et al.*, 1999b; *Munro et al.*, 1998] or a feed forward neural network algorithm [*Müller et al.*, 2003] provide good overall agreement with respect to sonde data (10% relative difference), although some finer structures in the lower stratosphere can hardly be reproduced. By comparison, the present work demonstrates that the thermal IR remote sounders offer better sensitivity in the troposphere and the lower stratosphere, with two independent pieces of information that can be retrieved below 25 km in most cases. The two resulting partial columns (ground to 12 km and 12–24 km) agree with the local sonde measurements to generally better than

10%, which is similar to the accuracy of the UV-visible instruments higher up. For high radiances, the thermal infrared instruments also provide information on ozone in the boundary layer. A synergetic use of both types of instruments, sounding the same air mass, is therefore expected to improve significantly the accuracy as well as the vertical sensitivity of the retrievals.

5. Conclusions

[35] The retrieval of ozone vertical profiles from a set of high-resolution FT nadir spectra recorded by the IMG instrument between December 1996 and June 1997 has been performed for the first time. The optimal estimation method was used in the retrievals, along with a priori information built from model climatologies. We have demonstrated that the IMG measurements contain between two and four independent pieces of information on the vertical ozone distribution, depending on the Earth's outgoing radiance. It was found that the sensitivity is maximal between 7 and 22 km. On the basis of the error analysis, it was concluded that the retrieval enables to reduce the uncertainty on the a priori ozone profile by a factor two to three, in the 5–40 km altitude range: The total error is dominated by the smoothing error, with additional contributions attributed to the measurement noise and the imperfect characterization of the temperature profile and of the ILS.

[36] The comparison of the retrieved ozone profiles with coincident sonde measurements, performed at seven representative sites, has revealed the potential of the satellite measurements to capture the spatial and temporal variations of the ozone content in the troposphere and in the stratosphere. In particular, it was shown that the profile retrievals allow the extraction of at least three ozone partial columns (ground to 12 km, 12 to 24 km and 24 km to higher altitudes), which agree with the sondes data to generally better than 10%. Especially the lower-stratospheric column (12–24 km) can be accurately retrieved from the IMG measurements. Most importantly, we have found that the trospospheric ozone amount is also well measured, except in the Southern Hemisphere, where it is characterized by low values. Based upon these results, it was demonstrated that the measurements contain sufficient information to reproduce the height variations of the stratospheric ozone layer between the different sites but also some finer variations in the ozone distribution. These include the observations of a secondary ozone maximum in the upper troposphere–lower stratosphere at northern midlatitudes and of the stratospheric ozone depletion events in the Arctic during springtime. The high sensitivity of the measurements to ozone in the free troposphere and the lower stratosphere is expected to make significant contribution to the understanding of STE.

[37] More generally, the results presented in this work have highlighted the scientific return to be expected from the operation of new generation space-borne infrared tropospheric sounders (e.g., TES/AURA and IASI/METOP). It is further foreseen that a synergetic use of IR and UV-visible instruments, which would take advantage of the better sensitivity of the IR measurements toward ozone in the troposphere and lower stratosphere and of the UV measurements higher up, will improve both the accuracy and the vertical resolution of the profile retrievals. This piece of research will bring essential information to get a better insight into the changing ozone distributions on the global scale.

[38] **Acknowledgments.** The research was funded by the Fonds National de la Recherche Scientifique (FNRS, Belgium), the Belgian State Federal Office for Scientific, Technical and Cultural Affairs and the European Space Agency (contract EV-1103C and ESA-Prodex arrangement C90-115). Financial support by the "Actions de Recherche Concertées" (Communauté Française de Belgique) is also acknowledged. This work was undertaken in the framework of the ISSWG (IASI Sounding Science Working Group) activities under the auspices of EUMETSAT (European Organization for the Exploitation of Meteorological Satellites) and CNES (Centre National d'Etudes Spatiales). The authors are grateful to IMGDIS/ERSDAC for providing the IMG level 1 data. Several data used in this publication were obtained as part of the Network for the Detection of Stratospheric Change (NDSC) and the World Ozone and Ultraviolet Radiation Data Centre (WOUDC) and are publicly available (see http://www.ndsc.ncep.noaa.gov, http://www.woudc.org/). Pierre-François Coheur is a Research Associate with the F.N.R.S. (Belgium).

References

Barret, B., D. Hurtmans, M. R. Carleer, M. De Mazière, E. Mahieu, and P. F. Coheur (2005), Line narrowing effect on the retrieval of HF and HCl vertical profiles from FTIR ground-based measurements, *J. Quant. Spectross. Radiat. Transfer*, *95*(4), 499–519.

Bowman, K. W., J. Worden, T. Steck, H. M. Worden, S. Clough, and C. Rodgers (2002), Capturing time and vertical variability of tropospheric ozone: A study using TES nadir retrievals, *J. Geophys. Res.*, *107*(D23), 4723, doi:10.1029/2002JD002150.

Brasseur, G. P., D. A. Hauglustaine, S. Walters, P. J. Rasch, J. F. Müller, C. Granier, and X. X. Tie (1998), MOZART, a global chemical transport model for ozone and related chemical tracers: 1. Model description, *J. Geophys. Res.*, *103*(D21), 28,265–28,289.

Burrows, J. P., et al. (1999), The global ozone monitoring experiment (GOME): Mission concept and first scientific results, *J. Atmos. Sci.*, *56*(2), 151–175.

Chédin, A., R. Saunders, A. Hollingsworth, N. Scott, M. Matricardi, J. Etcheto, C. Clerbaux, R. Armante, and C. Crevoisier (2003), The feasibility of monitoring CO_2 from high-resolution infrared sounders, *J. Geophys. Res.*, *108*(D2), 4064, doi:10.1029/2001JD001443.

Clerbaux, C., P. Chazette, J. Hadji-Lazaro, G. Mégie, J. F. Müller, and S. A. Clough (1998), Remote sensing of CO, CH_4, and O_3 using a spaceborne nadir-viewing interferometer, *J. Geophys. Res.*, *103*(D15), 18,999–19,013.

Clerbaux, C., J. Hadji-Lazaro, S. Payan, C. Camy-Peyret, and G. Mégie (1999), Retrieval of CO columns from IMG ADEOS spectra, *IEEE Trans. Geosci. Remote Sens.*, *37*(3), 1657–1661.

Clerbaux, C., J. Hadji-Lazaro, D. Hauglustaine, G. Mégie, B. Khattatov, and J. F. Lamarque (2001), Assimilation of carbon monoxide measured from satellite in a three-dimensional chemistry-transport model, *J. Geophys. Res.*, *106*(D14), 15,385–15,394.

Clerbaux, C., J. Hadji-Lazaro, S. Payan, C. Camy-Peyret, J. X. Wang, D. P. Edwards, and M. Luo (2002), Retrieval of CO from nadir remote-sensing measurements in the infrared by use of four different inversion algorithms, *Appl. Opt.*, *41*(33), 7068–7078.

Clerbaux, C., J. Hadji-Lazaro, S. Turquety, G. Mégie, and P. F. Coheur (2003), Trace gas measurements from infrared satellite for chemistry and climate applications, *Atmos. Chem. Phys.*, *3*, 1495–1508.

Clough, S. A., C. P. Rinsland, and P. D. Brown (1995), Retrieval of tropospheric ozone from simulations of nadir spectral radiances as observed from space, *J. Geophys. Res.*, *100*(D8), 16,579–16,593.

Clough, S. A., M. W. Shephard, E. Mlawer, J. S. Delamere, M. Iacono, K. Cady-Pereira, S. Boukabara, and P. D. Brown (2005), Atmospheric radiative transfer modeling: A summary of the AER codes, *J. Quant. Spectrosc. Radiat. Transfer*, *91*(2), 233–244.

Coheur, P. F., C. Clerbaux, and R. Colin (2003), Spectroscopic measurements of halocarbons and hydrohalocarbons by satellite-borne remote sensors, *J. Geophys. Res.*, *108*(D4), 4130, doi:10.1029/2002JD002649.

Coy, L., E. R. Nash, and P. A. Newman (1997), Meteorology of the polar vortex: Spring 1997, *Geophys. Res. Lett.*, *24*(22), 2693–2696.

Deeter, M. N., L. K. Emmons, D. P. Edwards, J. C. Gille, and J. R. Drummond (2004), Vertical resolution and information content of CO profiles retrieved by MOPITT, *Geophys. Res. Lett.*, *31*, L15112, doi:10.1029/2004GL020235.

Eichmann, K. U., K. Bramstedt, M. Weber, V. V. Rozanov, R. Hoogen, and J. P. Burrows (1999), O_3 profiles from GOME satellite data-II: Observa-

tions in the Arctic spring 1997 and 1998, *Phys. Chem. Earth*, *24*(5), 453–457.

Fishman, J., A. E. Wozniak, and J. K. Creilson (2003), Global distribution of tropospheric ozone from satellite measurements using the empirically corrected tropospheric ozone residual technique: Identification of the regional aspects of air pollution, *Atmos. Chem. Phys.*, *3*, 893–907.

Hadji-Lazaro, J., C. Clerbaux, and S. Thiria (1999), An inversion algorithm using neural networks to retrieve atmospheric CO total columns from high-resolution nadir radiances, *J. Geophys. Res.*, *104*(D19), 23,841–23,854.

Hadji-Lazaro, J., C. Clerbaux, P. Couvert, P. Chazette, and C. Boonne (2001), Cloud filter for CO retrieval from IMG infrared spectra using ECMWF temperatures and POLDER cloud data, *Geophys. Res. Lett.*, *28*(12), 2397–2400.

Hauglustaine, D. A., G. P. Brasseur, S. Walters, P. J. Rasch, J. F. Müller, L. K. Emmons, and C. A. Carroll (1998), MOZART, a global chemical transport model for ozone and related chemical tracers: 2. Model results and evaluation, *J. Geophys. Res.*, *103*(D21), 28,291–28,335.

Hoogen, R., V. V. Rozanov, K. Bramstedt, K. U. Eichmann, M. Weber, and J. P. Burrows (1999a), O-3 profiles from GOME satellite data-I: Comparison with ozonesonde measurements, *Phys. Chem. Earth*, *24*(5), 447–452.

Hoogen, R., V. V. Rozanov, and J. P. Burrows (1999b), Ozone profiles from GOME satellite data: Algorithm description and first validation, *J. Geophys. Res.*, *104*(D7), 8263–8280.

Jacquinet-Husson, N., et al. (1999), The 1997 spectroscopic GEISA databank, *J. Quant. Spectrosc. Radiat. Transfer*, *62*(2), 205–254.

Jacquinet-Husson, N., et al. (2005), The 2003 edition of the GEISA/IASI database, *J. Quant. Spectrosc. Radiat. Transfer*, *95*(4), 429–467.

Kauppinen, J., and P. Saarinen (1992), Line-shape distortions in misaligned cube corner interferometers, *Appl. Opt.*, *31*(1), 69–74.

Kobayashi, H., A. Shimota, K. Kondo, E. Okumura, Y. Kameda, H. Shimoda, and T. Ogawa (1999), Development and evaluation of the interferometric monitor for greenhouse gases: A high-throughput Fourier-transform infrared radiometer for nadir Earth observation, *Appl. Opt.*, *38*(33), 6801–6807.

Lelieveld, J., and F. J. Dentener (2000), What controls tropospheric ozone?, *J. Geophys. Res.*, *105*(D3), 3531–3551.

Li, D., and K. P. Shine (1995), A 4-dimensional ozone climatology for UGAMP model, *Internal Rep. 35*, U. K. Univ. Global Atmos. Modell. Programme, Reading, U. K.

Lubrano, A. M., G. Masiello, C. Serio, M. Matricardi, and R. Rizzi (2002), IMG evidence of chlorofluorocarbon absorption in the atmospheric window 800–900 cm^{-1}, *J. Quant. Spectrosc. Radiat. Transfer*, *72*(5), 623–635.

Müller, M. D., A. K. Kaifel, M. Weber, S. Tellmann, J. P. Burrows, and D. Loyola (2003), Ozone profile retrieval from Global Ozone Monitoring Experiment (GOME) data using a neural network approach (Neural Network Ozone Retrieval System (NNORSY)), *J. Geophys. Res.*, *108*(D16), 4497, doi:10.1029/2002JD002784.

Munro, R., R. Siddans, W. J. Reburn, and B. J. Kerridge (1998), Direct measurement of tropospheric ozone distributions from space, *Nature*, *392*(6672), 168–171.

Peters, W., M. C. Krol, J. P. F. Fortuin, H. M. Kelder, A. M. Thompson, C. R. Becker, J. Lelieveld, and P. J. Crutzen (2004), Tropospheric ozone over a tropical Atlantic station in the Northern Hemisphere: Paramaribo, Surinam, *Tellus, Ser. B*, *56*(1), 21–34.

Rodgers, C. D. (2000), *Inverse Methods for Atmospheric Sounding: Theory and Practice*, World Sci., Hackensack, N. J.

Rothman, L. S., et al. (2003), The HITRAN molecular spectroscopic database: Edition of 2000 including updates through 2001, *J. Quant. Spectrosc. Radiat. Transfer*, *82*(1–4), 5–44.

Thompson, A. M., et al. (2003a), Southern Hemisphere Additional Ozonesondes (SHADOZ) 1998–2000 tropical ozone climatology: 1. Comparison with Total Ozone Mapping Spectrometer (TOMS) and ground-based measurements, *J. Geophys. Res.*, *108*(D2), 8238, doi:10.1029/2001JD000967.

Thompson, A. M., et al. (2003b), Southern Hemisphere Additional Ozonesondes (SHADOZ) 1998–2000 tropical ozone climatology: 2. Tropospheric variability and the zonal wave-one, *J. Geophys. Res.*, *108*(D2), 8241, doi:10.1029/2002JD002241.

Thompson, A. M., J. C. Witte, S. J. Oltmans, and F. J. Schmidlin (2004), Shadoz—A tropical ozonesonde-radiosonde network for the atmospheric community, *Bull. Am. Meteorol. Soc.*, *85*(10), 1549–1564.

Turquety, S., J. Hadji-Lazaro, and C. Clerbaux (2002), First satellite ozone distributions retrieved from nadir high-resolution infrared spectra, *Geophys. Res. Lett.*, *29*(24), 2198, doi:10.1029/2002GL016431.

Turquety, S., J. Hadji-Lazaro, C. Clerbaux, D. A. Hauglustaine, S. A. Clough, V. Cassé, P. Schlüssel, and G. Mégie (2004), Operational trace gas retrieval algorithm for the Infrared Atmospheric Sounding Interferometer, *J. Geophys. Res.*, *109*, D21301, doi:10.1029/2004JD004821.

B. Barret, P.-F. Coheur, and D. Hurtmans, Spectroscopie de l'Atmosphère, Service de Chimie Quantique et de Photophysique, Université Libre de Bruxelles, B-1050 Brussels, Belgium. (pfcoheur@ ulb.ac.be)

C. Clerbaux, J. Hadji-Lazaro, and S. Turquety, Service d'Aéronomie, Institut Pierre-Simon Laplace, F-75252 Paris, France.